INT. J. NUM. METH. HEAT FLUID FLOW, VOL. 6 NO. 5, 49–62 (1996)

NUMERICAL SOLUTION OF THE THERMALLY-ASSISTED DIFFUSION OF HYDROGEN IN ZIRCONIUM ALLOYS CONSIDERING HYSTERESIS AND FINITE-RATE KINETICS

GUSTAVO C. BUSCAGLIA AND RAÚL A. ENRIQUE

Centro Atómico Bariloche and Instituto Balseiro, (8400) Bariloche, Rio Negro, Argentina

ABSTRACT

Presents a new method for the numerical simulation of diffusion with phase-change. The method is able to handle hysteresis and finite-rate kinetics in the phase-change reaction. Such phenomena are frequent in solid-solid phase transitions. The model problem discussed concerns hydrogen migration and hydride precipitation in zirconium and its alloys, a problem of interest to the nuclear industry. With respect to previous ones, our method is the first to incorporate an implicit treatment of diffusion, thus avoiding mesh-dependent stability limits in the time step. The CPU time can in this way be reduced by a factor of 10-20 in applications. Addresses, through numerical studies, convergence with respect to mesh refinement and reduction of the time step. Also reports on an application of the method to the simulation of laboratory experiments. Shows that the method is a powerful tool to deal with general phase-change problems, extendable to other physical systems.

KEY WORDS Hydrogen migration Zirconium hydride Hydride blisters Phase-change problem Hysteresis Finite-rate kinetics Stefan problem Numerical simulation Finite elements Implicit scheme

INTRODUCTION

The interaction of hydrogen with zirconium and its alloys leads to a physical and mathematical problem that serves as a paradigm to many other phase transitions, in particular to those occurring in the solid state. As an impurity, the mobility of H atoms in Zr (a metal with hexagonal structure) is rather high, and its migration can be modelled accurately as a diffusion process. In the presence of a non-homogeneous thermal field, however, the thermal gradient appears under the form of a convective term added to the diffusion equations, causing higher concentrations to appear where the temperature is lower. This phenomenon is known as thermally-assisted diffusion.

The solubility of H in metallic Zr is nevertheless limited, and when it exceeds the (temperature dependent) terminal solid solubility (*TSS*) the hexagonal matrix undergoes a phase transition and a new phase precipitates: the zirconium hydride, $ZrH_{1.5}$ (a face-centred cubic structure much richer in hydrogen)[1]. Up to this point, the typical structure of a Stefan problem can be identified as the existence of two phases (metal and hydride), with diffusion within each phase and the H concentration discontinuous between them. In the case of the solidification of a pure substance, the variable obeying a diffusive process is the temperature and the discontinuous variable is the specific enthalpy (the height of the discontinuity being the latent heat).

Solid-solid phase transitions involve other phenomena that can be viewed as generalizations of the Stefan problem. First, the *TSS* is experimentally observed to depend on whether the

0961–5539/96
© 1996 MCB University Press Ltd

Received June 1995
Revised August 1995

© Emerald Backfiles 2007

concentration is increasing or decreasing. In other words, if the H concentration in the metal is *TSSP* (*TSS* for precipitation) when hydrides begin to precipitate, in order to dissolve existing hydrides the concentration of H in the metallic matrix must be lowered to *TSSD* (*TSS* for dissolution). As $TSSD < TSSP$ this is a typical hysteresis phenomenon. The analogy with the solidification of a pure substance would imply that the solid→liquid transition occurs at a higher temperature than that of the liquid→solid. Hysteresis in the zirconium-hydrogen system has been observed in experiments of Erickson and Hardie[2] and of Slattery[3]. It has been explained as a consequence of elastic-plastic accommodation between the metal and the hydride by Puls[4] (see also[5]).

In addition, in many solid-state phase transitions the kinetics of the reaction cannot be considered instantaneous. Both the metal→hydride and the hydride→metal reactions occur at a finite rate that is a function of the oversaturation or undersaturation of the metallic matrix. If the concentration C_α in the metal exceeds *TSSP*, then hydrides precipitate at a rate proportional to the difference $C_\alpha - TSSP$, and if C_α is lower than *TSSD* existing hydrides dissolve at a rate proportional to $TSSD - C_\alpha$. We refer only to what happens in the metallic (α-phase) because the concentration of H in the hydride (δ-phase, a chemical compound) will be considered fixed, C_δ= 16,000 ppm (parts per million expressed by weight).

In this paper we describe a novel methodology for the numerical solution of phase-change problems, taking into account both hysteresis effects and finite-rate kinetics. Though we will apply it to hydrogen migration in zirconium and its alloys, it can be readily extended to several other phase-change problems. Our method, like many others available for the Stefan problem, incorporates an implicit treatment of the diffusion term, which is essential to avoid mesh-dependent limits in the time-step size.

THE MODEL PROBLEM: HYDROGEN MIGRATION IN Zr

The basic model of thermally-assisted diffusion of hydrogen in zirconium alloys is based on the following assumptions[6-8]:

- Hydrogen diffusion occurs only in the α-phase (metal matrix), according to linear transport equations. This simplification is introduced because the diffusion coefficient of the δ-phase (hydride) is much lower than that of the α-phase.
- All quantities are considered macroscopically, and suitable spatial homogenization is performed.
- The precipitation or dissolution of hydrides is a local phenomenon, viewed in the model as a variation of the volumetric fractions of the α- and δ-phases.

As a result of the homogenization procedure we have, as functions of position and defined in *all* the domain, the total hydrogen concentration C, the hydrogen concentration in the α-and δ-phases C_α and C_δ, and the volumetric fraction of α-phase, v_α. These quantities are related by the lever

$$C = v_\alpha C_\alpha + (1 - v_\alpha) C_\delta = v_\alpha (C_\alpha - C_\delta) + C_\delta. \tag{1}$$

In this way any point of the domain Ω can be in one of three possible states: pure α-phase ($v_\alpha = 1$), coexistence of phases ($0 < v_\alpha < 1$, similar to the mushy zone in binary alloys solidification) or pure δ-phase ($v_\alpha = 0$). The homogenization procedure also applies to the diffusion coefficient D, because precipitated hydrides obstruct the hydrogen flux. The effective diffusion coefficient is assumed to be equal to the diffusion coefficient multiplied by the volumetric fraction v_α.

Finite-rate kinetics allows us to describe the phase-change with a differential equation[9]. The equation we present below is a generalization[10] of the proposal of Marino[11], so as to consider all possible values for the volumetric fraction v_α.

© Emerald Backfiles 2007

The previous considerations lead to the following statement of the problem:

Given $C(\bullet, 0)$, $C_\alpha(\bullet, 0)$, (and therefore $v_\alpha(\bullet, 0)$) in Ω, find the evolution of these quantities at all times $t > 0$, according to the following governing equations:

$$\frac{\partial C}{\partial t} = div\{Dv_\alpha(\nabla C_\alpha + \frac{Q^* C_\alpha}{RT^2}\nabla T)\} + q \tag{2}$$

$$\frac{\partial v_\alpha}{\partial t} = -\frac{\alpha^2 v_\alpha^p}{(C_\delta - C_\alpha)} F(C_\alpha) \tag{3}$$

with:

$$F(C_\alpha) = \begin{cases} C_\alpha - TSSP \text{ if } C_\alpha > TSSP \text{ and } v_\alpha > 0 \\ C_\alpha - TSSD \text{ if } C_\alpha > TSSD \text{ and } v_\alpha < 1 \\ 0 \qquad \text{otherwise} \end{cases}$$

where Equation (2) is the conservation equation for hydrogen (notice the diffusion term $div(Dv_\alpha \nabla C_\alpha)$, the convective-like term $div(Dv_\alpha Q^* C_\alpha \nabla T/(RT^2))$ and the volumetric source q), and Equation (3) is the local law for the precipitation-dissolution reaction (F is a measure of the oversaturation or undersaturation of the α-phase and thus vanishes if C_α lies between *TSSD* and *TSSP*; the exponent p depends on the geometric distribution of the precipitated hydrides). In principle, α could be different for precipitation and dissolution, but we have not considered this in the model because of lack of experimental data.

The governing equations take a simpler form changing the variables as proposed by Byrne[12]. With

$$E = e^{Q^*/RT} \tag{4}$$

and defining the following overlined variables

$$\begin{aligned} \overline{C} &= e^{-Q^*/RT} C = E^{-1} C \\ \overline{C}_\alpha &= e^{-Q^*/RT} C_\alpha = E^{-1} C_\alpha \\ \overline{C}_\delta &= e^{-Q^*/RT} C_\delta = E^{-1} C_\delta \\ \overline{TSSD} &= e^{-Q^*/RT} TSSD = E^{-1} TSSD \\ \overline{TSSP} &= e^{-Q^*/RT} TSSP = E^{-1} TSSP \end{aligned} \tag{5}$$

the set of equations (2) and (3) takes the form:

$$E\frac{\partial \overline{C}}{\partial t} = div(ED v_\alpha \nabla \overline{C}_\alpha) + q \tag{6}$$

$$\frac{\partial v_\alpha}{\partial t} = -\frac{\alpha^2 v_\alpha^p}{(\overline{C}_\delta - \overline{C}_\alpha)} \overline{F}(\overline{C}_\alpha) \tag{7}$$

with:

$$\overline{F}(\overline{C}_\alpha) = \begin{cases} \overline{C}_\alpha - \overline{TSSP} \text{ if } \overline{C}_\alpha > \overline{TSSP} \text{ and } v_\alpha > 0 \\ \overline{C}_\alpha - \overline{TSSD} \text{ if } \overline{C}_\alpha < \overline{TSSD} \text{ and } v_\alpha < 1 \\ 0 \qquad \text{otherwise} \end{cases}$$

where we have assumed that the temperature field does not vary with time.

© Emerald Backfiles 2007

THE NUMERICAL METHOD

The numerical method is based on a splitting of each time-step. In the first substep diffusion is allowed but preventing phase change from occurring, i.e. fixing the value of v_α. In this way we obtain a new hydrogen distribution. In the second part we advance the precipitation-dissolution reaction pointwise, according to the kinetic equation and the phase diagram. This scheme could therefore be classified as a "middle point scheme" (see the recent review by Idelsohn *et al.*[13]; an example of this kind of scheme is that proposed by Pham[14]).

First substep: diffusion

Given the values $\bar{C}^n$, $\bar{C}^n_\alpha$, v^n_α (algorithmic approximations of the corresponding fields) at time t^n, hydrogen diffusion is allowed during a lapse equal to Δt, but inhibiting phase change. Then, during this substep

$$\frac{\partial v_\alpha}{\partial t} = 0 \tag{8}$$

holds. Making use of the time derivative of the lever-rule equation (1), we can transform the conservation equation (6) into:

$$E\frac{\partial \bar{C}}{\partial t} = Ev_\alpha(x,t^n)\frac{\partial \bar{C}_\alpha}{\partial t} = div\{E\,D\;\; v_\alpha(x,t^n)\nabla \bar{C}_\alpha\} + q \tag{9}$$

where we have made use of the fact that $\bar{C}_\delta$ does not depend on time. Taking $\bar{C}_\alpha$ as the unknown variable, this formulation allows for the use of a backward scheme for the diffusion part. This is a crucial improvement with respect to the forward scheme presented by Byrne[9], which suffers from the well-known stability limits of forward treatments of diffusion problems. Our backward scheme reads:

$$E\;\; v_\alpha(x,t^n)\frac{\bar{C}_\alpha^{n+\frac{1}{2}} - \bar{C}_\alpha^n}{\nabla t} = div\{E\,D\;\; v_\alpha(x,t^n)\nabla \bar{C}_\alpha^{n+\frac{1}{2}}\} + q \tag{10}$$

and the variational equation can be rapidly obtained by the standard Galerkin procedure:

$$\frac{1}{\Delta t}\int_\Omega E\;\; v^n_\alpha(\bar{C}_\alpha^{n+\frac{1}{2}} - \bar{C}^n_\alpha)N_i\, d\Omega + \int_\Omega DEv^n_\alpha \nabla \bar{C}_\alpha^{n+\frac{1}{2}}\nabla N_i\;\; d\Omega - \int_{\partial\Omega} hN_i\;\; dS - \int_\Omega qN_i\;\; d\Omega = 0 \tag{11}$$

for every test function N_i, where h stands for the hydrogen flux through the boundary. In this way, we obtain a "predictor" value for the hydrogen concentration in solid solution, $\bar{C}^{n+1/2}_\alpha$, and the corresponding new total hydrogen distribution, $\bar{C}^{n+1/2}$ given by

$$\bar{C}^{n+\frac{1}{2}} = v^n_\alpha(\bar{C}_\alpha^{n+\frac{1}{2}} - \bar{C}_\delta) + \bar{C}_\delta. \tag{12}$$

In the general situation, the assumption made in this substep that v_α is fixed is not consistent with the kinetic equation (7). The second substep is needed to consider phase-change processes.

Second substep: phase-change

The first substep is used to update the total concentration field, which will remain unchanged during this second substep as the evolution towards equilibrium will be performed locally; that is $\bar{C}^{n+1} = \bar{C}^{n+1/2}$. At any point, the change in total hydrogen concentration during the time step, $\Delta\bar{C} = \bar{C}^{n+1} - \bar{C}^n$, affects, at the beginning of this second substep, only the α phase. Typically, this

© Emerald Backfiles 2007

will lead to concentrations $\bar{C}_\alpha^{n+1/2}$ in this phase that cause the precipitation or dissolution of hydrides, a process that is accounted for in this second substep. As the rate of change of the total concentration during the time step is known from the previous substep, we can combine the time derivative of Equation (1) with Equation (7) to get

$$\alpha^2 v_\alpha^p \bar{F}(\bar{C}_\alpha) + v_\alpha \frac{\partial \bar{C}_\alpha}{\partial t} = \frac{\partial \bar{C}}{\partial t} \tag{13}$$

where the right-hand side is known. In other words, we have the following equation for $\bar{C}_\alpha$

$$v_\alpha^n \frac{\partial \bar{C}_\alpha}{\partial t} = \frac{\bar{C}^{n+1} - \bar{C}^n}{\Delta t} - \alpha^2 (v_\alpha^n)^p \bar{F}(\bar{C}_\alpha) \tag{14}$$

which will be solved at each node of the mesh, as it involves no spatial derivatives. In Equation (14) an explicit treatment of v_α has been adopted; this does not lead to significant errors because, as C_δ is very large, v_α changes much more slowly than C_α. The initial condition of this ordinary differential equation at each node is $\bar{C}^{n+1/2}$, and it must be solved during a time interval equal to a complete time step Δt. Moreover, since $\bar{F}$ is a piecewise linear function of $\bar{C}_\alpha$, this equation can be solved analytically. This is important because it prevents the appearance of spurious negative values of v_α which would lead to negative effective diffusivities in the next step.

To do this we separate all the possible conditions in the options for $\bar{F}$. As a simplification, our analysis of the possible cases will only consider the "predictor" values $\bar{C}_\alpha^{n+1/2}$ (note that this simplification is not essential to the method we are presenting).

Remark 1: Notice that Equation (10) becomes ill-posed if v_α takes the zero value somewhere within the domain. This corresponds to a pure δ-phase region that can indeed occur (both in our model and in laboratory experiments[15]). In the limit $\alpha^2 \to \infty$ (instantaneous kinetics) the exact solutions to the model exhibit regions where v_α is strictly zero[9,16]. If $\alpha^2 < \infty$ (finite-rate kinetics) v_α tends asymptotically to zero in some regions and again Equation (10) becomes ill-posed. Of course this is not a problem of the model, as Equation (9) clearly states that the total concentration in such regions must remain fixed at the value C_δ and, as no α-phase is present, C_α is irrelevant. The problem comes from our use of the time derivative of the lever rule (1) to get Equation (10). This use is not correct if v_α is zero. However, as this is essential to obtain a backward scheme (in fact, it is the key idea of our method), we avoid this difficulty imposing a lower bound ε for v_α. In the detailed description of our algorithm presented below, it can be seen that we stop the phase-change when v_α^n reaches the value of ε. Our numerical experiments have conclusively shown that this modification of the model does not affect the solution whenever ε is lower than 10^{-2}.

Defining a nodal *characteristic time* $\tau = 1/(v_\alpha^n)^{p-1}\alpha^2$, the second substep procedure to apply at each node is the following:

Part 1: obtaining $\bar{C}_\alpha^{n+1}$:

(1) Case 1 (precipitation): if $\bar{C}_\alpha^{n+1} > \overline{TSSP}$ and $v_\alpha^n > \varepsilon$ then

- If $\bar{C}_\alpha^n > \overline{TSSP}$ precipitation occurs during all the time-step, thus put

$$\bar{C}_\alpha^{n+1} = \overline{TSSP} + (\bar{C}_\alpha^n - \overline{TSSP}) e^{-\Delta t/\tau} + \frac{\Delta \bar{C}}{\Delta t} \frac{\tau}{v_\alpha^n} (1 - e^{-\Delta t/\tau}). \tag{15}$$

- If $\bar{C}_\alpha^n < \overline{TSSP}$, it will also be assumed that precipitation takes place during the complete time-step, setting $\bar{C}_\alpha^n = TSSP$, and then using (15).

(2) Case 2 (dissolution): if $\bar{C}_\alpha^{n+1/2} < \overline{TSSD}$ and $v_\alpha^n < 1$ then

- If $\bar{C}_\alpha^n < \overline{TSSD}$, then

© Emerald Backfiles 2007

$$\overline{C}_\alpha^{n+1} = \overline{TSSD} + (\overline{C}_\alpha^n - \overline{TSSD}) e^{-\Delta t/\tau} + \frac{\Delta \overline{C}}{\Delta t} \frac{\tau}{v_\alpha^n} (1 - e^{-\Delta t/\tau}). \tag{16}$$

- If $\overline{C}_\alpha^n > \overline{TSSD}$ it will be assumed that dissolution takes place during the complete time-step, setting $\overline{C}_\alpha^n = \overline{TSSD}$, and then using (16).

(3) Case 3 (no phase change): in all the other cases, no phase-change occurs and thus:

$$\overline{C}_\alpha^{n+1} = \overline{C}_\alpha^{n+\frac{1}{2}}. \tag{17}$$

Remark 2: In the case of instantaneous kinetics ($\alpha \to \infty \Rightarrow \tau \to 0$), we use the same procedure as before replacing Equations (15) and (16) by the appropriate expressions in this limit (which are just the solubility values, $\overline{TSSP}$ and $\overline{TSSD}$ respectively).

Part 2: obtaining v_α^{n+1}. The updated value for the nodal volumetric fraction comes from the lever rule as:

$$v_\alpha^{n+1} = \frac{\overline{C}^{n+1} - \overline{C}_\delta}{\overline{C}_\alpha^{n+1} - C_\delta} \tag{18}$$

Summary of the numerical procedure and comments

Although the numerical procedure presented above might seem quite involved, it can be shown that it is in fact simple, physically based, and mimics the processes that actually occur. To advance one time-step, we begin by solving Equation (11), a classical finite element problem where a mass matrix and a diffusion matrix can be identified. Solving Equation (11) we are diffusing the hydrogen through α-phase as if the δ-phase did not react with it. This is physically sound, because our model assumes that no diffusion occurs in the δ-phase. It should be clear that any numerical method (finite differences, finite volumes, etc.) could be used to solve the diffusion problem. Next, we determine node by node whether the resulting concentrations in the α-phase would produce phase-change, and determine through Equations (15) to (17) what concentration will be left in the α-phase. This is again in correspondence with the physics of the model, as the chemical reaction between phases is considered locally. Finally, Equation (18) is just an algebraic relation to keep the volumetric fraction of α-phase updated. The main advantage of our splitting is that it allows for an implicit treatment of diffusive terms. The time-step is thus only limited by accuracy considerations (see "Numerical tests (one-dimensional)" and not by numerical instability, as happens with explicit schemes.

NUMERICAL RESULTS: TESTS AND APPLICATION

The investigation of the thermally-assisted diffusion of hydrogen in zirconium was initiated as a response to a demand from the nuclear industry. In 1983, a pressure tube failed at the Pickering unit 2. The failure was produced by the growth of a pure hydride zone (or *blister*) in a cold spot, caused by a pressure-tube calandria-tube contact[17]. For this reason, a reliable model and a proper scheme for numerical simulations were needed. Although materials used in the nuclear industry are zirconium alloys (Zry-2, Zry-4, Zr-2.5% Nb), as far as thermodiffusion is concerned, the behaviour of the system is the same as for pure zirconium.

The numerical examples we will show here are taken from the work we have been carrying out for the experimental validation of the model and prediction of blister growth in pressure tubes of nuclear reactors[10,15,18]. In these numerical examples, we will pay special attention to the case of instantaneous kinetic, i.e. $\alpha^2 \to \infty$, because we have found that finite-rate kinetics does not play an important role in the physical situations of interest.

© Emerald Backfiles 2007

We will consider thermodiffusion of hydrogen in Zry-2 and in Zr-2.5% Nb. In the way it was stated, the algorithm serves for multidimensional cases. For the sake of simplicity, the cases under consideration will be either one-dimensional or axisymmetrical. Regarding the parameters of the materials, both the diffusivity and the terminal solid solubilities are functions of temperature through Arrhenius-type laws:

$$D = D_0\, e^{-Q/RT} \qquad TSSD = K_D\, e^{-H_D/RT} \qquad TSSP = K_P\, e^{-Hp/RT}$$

The heat of transport, Q^*, is a constant independent of temperature. Table 1 summarizes Zry-2 and Zr-2.5% Nb material parameters.

Table 1 Parameters of the material for zirconium alloys[9,19,20].

		Zry-2	Zr-2.5%Nb	
Frequency factor	D_0	0.217	0.41	mm^2/s
Activation energy	Q	36581	38400	J/mol
Dissolution constant	K_D	51700	60500	ppm
Precipitation constant	K_P	31437	41000	ppm
Heat of mixing (dissolution)	H_D	85000	33300	J/mol
Heat of mixing (precipitation)	H_P	31813	28000	J/mol
Heat of transport	Q^*	25116	20930	J/mol
Gas constant	R	8.314		J/Kmol

Numerical tests (one-dimensional)

We will first check the algorithm in a one-dimensional example, with instantaneous kinetics. The physical situation is taken from Sawatzky's experiments[8]. In those experiments, two 25mm rods of Zry-2 were charged with hydrogen, and a constant thermal gradient was imposed in the axial direction, by fixing the maximum and minimum temperature at the ends of the rod.

To demonstrate the convergence of the algorithm, *Figure 1* shows the superposition of the solutions computed on meshes with different refinements. The time simulated is one day. The initial condition is a homogeneous hydrogen concentration of 130ppm. Meshes with 100, 200 and 500 equal linear elements were used. The temperatures at the ends of the rod are 130°C (left) and 477°C (right). Thermally-assisted hydrogen diffusion in a two-phase regime has very particular characteristics as the reader can notice from the figure. The two-phase zone is situated on the left part, separated by a discontinuity in concentration (that spontaneously appears and moves with time; in *Figure 1* its position is $x \cong 15.8$mm) from an α-phase region. The actual form of the concentration profile can be explained from the underlying physics, but that would exceed the scope of this paper.

In *Figure 2* we show the convergence rate with spatial mesh refinement, h. That figure is a log-log plot of the mean square error (MSE) as a function of h, the length of the elements. To compute the MSE, we took as a reference the solution C_{ref} computed in a 500-element mesh. MSE is defined as

$$\mathrm{MSE} = \frac{1}{\sqrt{25}}\left[\int_0^{25}(C - C_{ref})^2\,dx\right]^{\frac{1}{2}} \tag{19}$$

From *Figure 2* a linear dependence of the L^2-norm of the error with h can be estimated. The non-monotonous dependence of the error with h is quite easy to explain: As the error is concentrated at discontinuities (see *Figure 1*), those meshes that provide better approximations near the discontinuities (i.e. those for which the discontinuity falls near the centre of an element) will lead

© Emerald Backfiles 2007

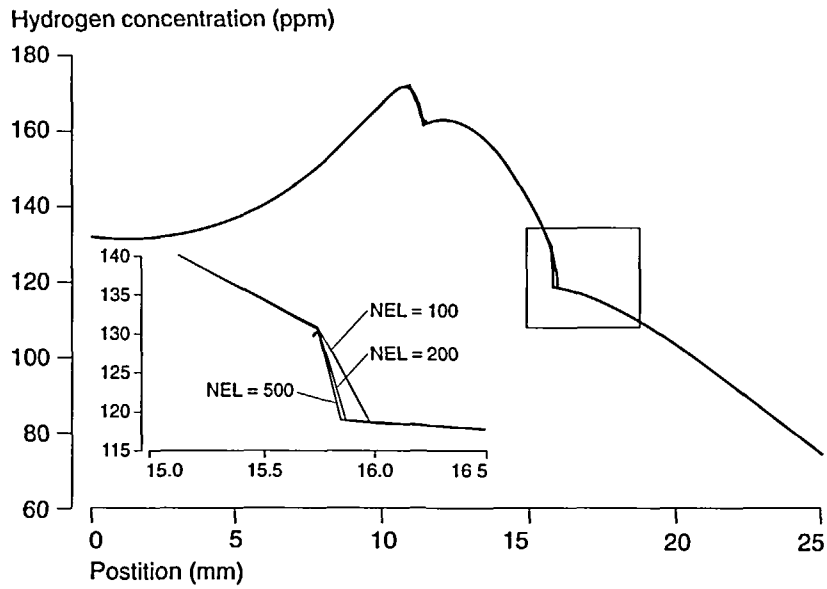

Figure 1 Numerical solutions in meshes with 100, 200 and 500 equal linear elements. The profile corresponds to the redistribution of an initially uniform hydrogen concentration of 130ppm, in a linear thermal field going from 130°C at the left (cold) end to 477°C at the right end. Parameters of the material correspond to Zry-2 (Sawatzky's experiments) and the simulation time is one day. Solutions are indistinguishable except locally at discontinuities of the exact solution (enlarged). The graph shows convergence of the proposed method

to smaller errors. This results in the wavy dependence shown in *Figure 2*. The h-values that correspond to these "fortunate" meshes would of course change if the error were measured at some other time, at which the discontinuities would have moved.

The semi-implicit method presented here is unconditionally stable, there is no upper limit for the time-step. As expected, increasing the time-step leads to a less accurate numerical solution. In *Figure 3* we plot the MSE of the final solution as a function of the time-step. The graph also shows the MSE for the fully-explicit algorithm([9,10], dashed lines). The stability limit for the explicit method is marked by the arrows. This figure shows the possibility of using longer time steps with our method than with that of 9, without an important loss of accuracy. For example, for the 200-element mesh, if we accept an error twice the error as $\Delta t \to 0$ for the given spatial discretization, then we can extend the time step by a factor of 30. The advantage of the implicit scheme grows as the mesh is refined, and also as we study processes with longer characteristic times, because our implicit method looses accuracy only when the time step becomes comparable with such times. In the application reported in the following section, our method consumes less CPU than the explicit one by a factor of at least 3.

Finally, *Figure 4* shows the effect of the kinetics on the hydrogen concentration profile at the end of the experiment (i.e. 34 days). The graph shows numerical solutions for evolution of the system. The parameter p chosen is 0, but we have observed that its value is unimportant, because the volumetric fraction v_α in this example is, everywhere, very close to 1.

Application to a 2D experimental situation

The physical situation corresponds to the experiment reported in Domizzi *et al.*[15], in which the authors were involved. The experiment consisted in producing a cold spot in a hydrogen-charged (cylindrical) Zr-2.5% Nb specimen. In this condition, it was experimentally observed that a pure-hydride region or blister grows in the cold zone. A detailed description of the experiment can be found in the reference.

© Emerald Backfiles 2007

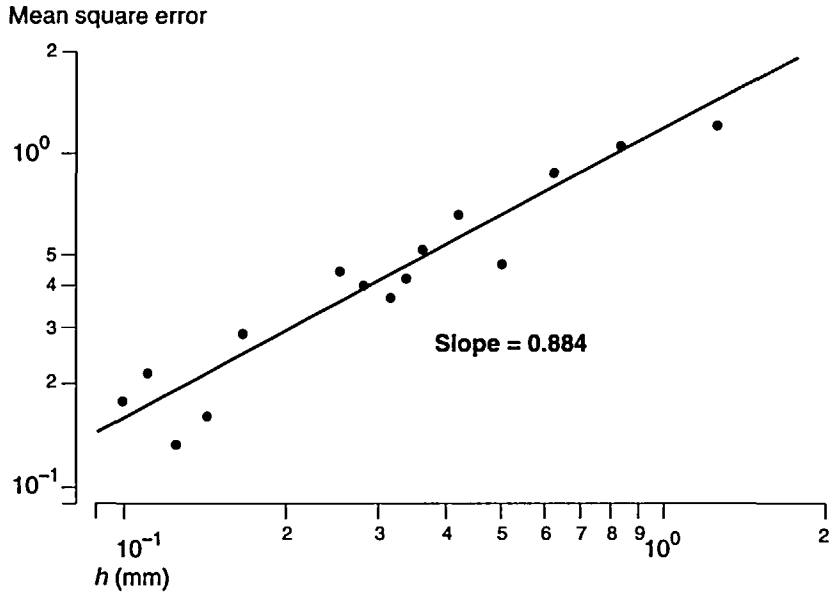

Figure 2 Mean square error (MSE) in ppm as function of the space refinement, h. The mean square error was calculated for different meshes taking as exact solution that computed on a 500 elements mesh ($h = 0.05$). Notice that even for coarse meshes ($h = 1.25$, 20 elements) MSE is approximately 1ppm, while the average concentration is 130ppm

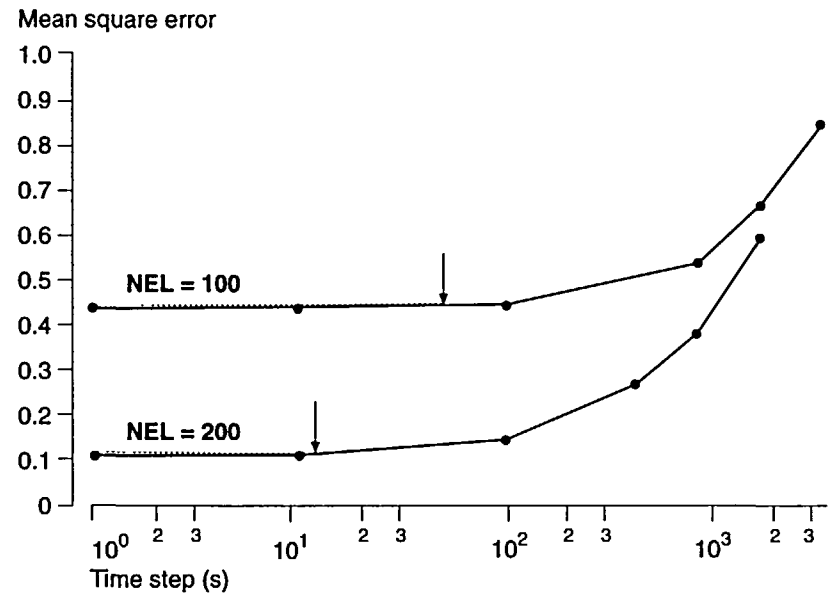

Figure 3 Mean square error (in ppm) as a function of the time step. The solid line corresponds to the implicit scheme and the dashed line to the fully explicit scheme[9,10]. The stability limit of the latter is marked by the arrows. This graph shows the possibility of extending the time step for the proposed method without an important loss of accuracy

© Emerald Backfiles 2007

The cold spot was produced by pressing an aluminium finger refrigerated by water on the central upper surface of the sample. The sample was, at the same time, kept over an aluminium block at 414°C. In this way, a very localized cold zone of ~ 200°C was created in a sample with an average temperature of 360-390°C. The thermal field, found solving an inverse problem from the experimental (readings at thermocouples) data, is shown in *Figure 5*. The samples had a radius of 17.5mm and a thickness of 3.9mm, and the initial (homogeneous) hydrogen concentration was around 300ppm. In these conditions, experiments of blister growth were carried out with times ranging from 1×10^5 seconds (~ 1 day), to 6×10^5 seconds (~ 7 days).

To solve the problem we used the meshes shown in *Figure 6*. These meshes have the required refinement in the cold zone for proper simulation of blister growth. The first mesh (STR), is a structured mesh with 9,000 bilinear elements, while the second one (UNSTR) has 1,921 linear triangular elements. With these meshes we computed the solution during 6×10^5 sec, with a time step of 200 sec for mesh STR and of 100 sec for mesh UNSTR. The numerical solutions are plotted in *Figure 7*.

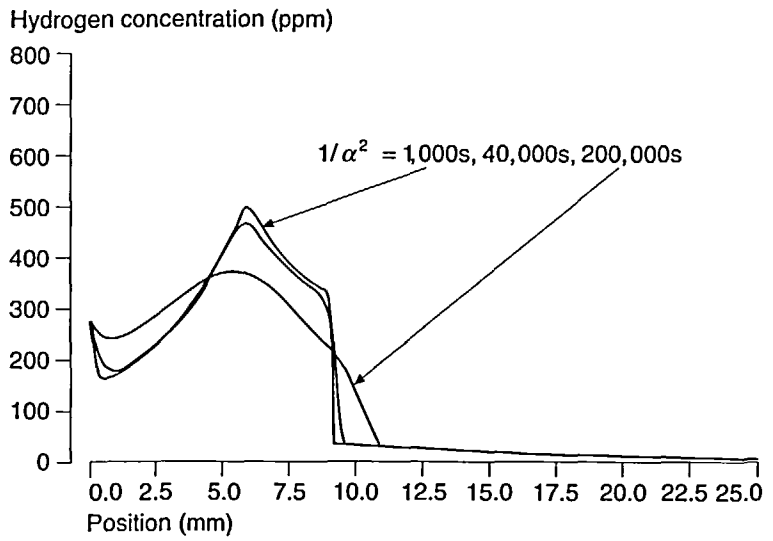

Figure 4 Solution of the problem at 34 days for different values of the kinetic coefficient. The parameter p was set equal to zero. This does not appreciably affect the numerical results for the volumetric fraction v_a in this problem is very close to 1

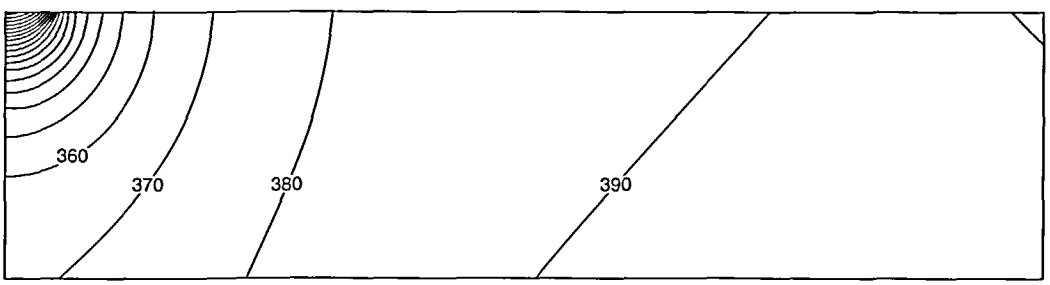

Figure 5 Thermal field in the sample in the Domizzi *et al.*[15] experiment. The problem is axisymmetric. Horizontal direction corresponds to radial direction and vertical direction to axial direction. Contour lines are plotted in an interval of 10°C from 390°C to 180°C. A localized cold spot in the upper central part of the sample can be appreciated

© Emerald Backfiles 2007

The numerical solutions of the problem show a very high hydrogen concentration in the cold zone (12,000-16,000ppm). As we move towards the hottest parts of the sample, the hydrogen concentration lowers rapidly to a value close to the initial concentration (200~400ppm). This calculated concentration field is the expected result, as the analysis of the exact solution of the model predicts a hydride blister (16,000 ppm) growing from the cold spot, followed by a discontinuity in the hydrogen concentration to a value close to the initial one[16]. Furthermore, these results are in qualitative and quantitative agreement with experimental data[15]. The numerical solution converges with mesh refinement, the results in *Figure 7* are obtained with meshes refined so as to obtain the desired accuracy.

Two discontinuity lines are present in the solution. One that separates the blister (pure δ-phase) from the coexistence zone ($\alpha + \delta$), and another that separates this coexistence zone from the solid solution (pure α-phase) zone. The saw-like aspect of the $C = 250$ and $C = 300$ppm contours in *Figure 7b* occurs because the decision concerning the boundaries of these zones is taken nodally (through the different cases in the phase-change section of the numerical method (Equations (15-17)). The method works equally well on both structured and unstructured meshes, and this saw-like aspect of the contours at discontinuities also occurs on structured meshes, though it cannot be appreciated in *Figure 7a* because the mesh is very fine. The mesh-following aspect of contours at discontinuities in structured meshes is illustrated in *Figure 8* with a rather coarse mesh. The cure is obviously to refine the mesh if any of the discontinuities of interest is poorly approximated by the method.

Finally, we should mention that one important effect of enlarging the time step is to smear out discontinuities. This can be observed comparing *Figures 7a* ($\Delta t = 200$ sec) and *7b* ($\Delta t = 100$ sec). In the latter the discontinuity in concentration at the blister boundary is more accurately predicted, not because the mesh is finer, but because the time step is smaller.

FINAL REMARKS

We have presented a numerical method for the solution of a phase-change problem that is able to handle several phenomena that appear in solid-solid line phase transitions. The model problem we have discussed applies to hydrogen migration and hydride precipitation in zirconium alloys, and is a slight generalization of that proposed by Byrne and Léger[9]. Previous methods for this problem[9,12,16,19,21] did not consider such phenomena, with the exception of that of Reference 9. The advantage of our method with respect to that of Reference 9 is that we handle the diffusion implicitly. As is well known, this avoids the appearance of mesh-dependent stability limits in the step size. Moreover, as shown in Reference 10, the numerical solutions obtained with our scheme are free of small oscillations that appear when using the *explicit* method of Reference 9 in fine meshes (also used in Reference 20 and, by the authors in References 10 and 15. The gain in computer time of an implicit treatment of diffusion increases as the mesh is refined and as the simulated time is longer. The simulation of the experiment reported in the previous section (167 hours of real time) took 36 hours of a SUN IPX with the explicit scheme on mesh STR, while with our method, on the same mesh, this time reduced to 12 hours. Also, as our method works as well on unstructured meshes, we were able to perform the simulation on the locally refined mesh UNSTR, with excellent results and a CPU time of 90 minutes. As an example of this gain in technological problems, we have recently simulated blister growth in reactor operating conditions, a process implying the simulation of 30 years of real time[18]. With the method presented here this simulation took 36 hours on a SPARC-10 (~80 hours of a SUN IPX) using a structured mesh, while with the explicit method, the same simulation would have taken 15 CPU days.

The splitting carried out in our method and the way we arrive to an implicit treatment of diffusion can easily be understood from a physical interpretation of the system. In addition, the extension to many other phase-change problems is quite straightforward. The same splitting can

© Emerald Backfiles 2007

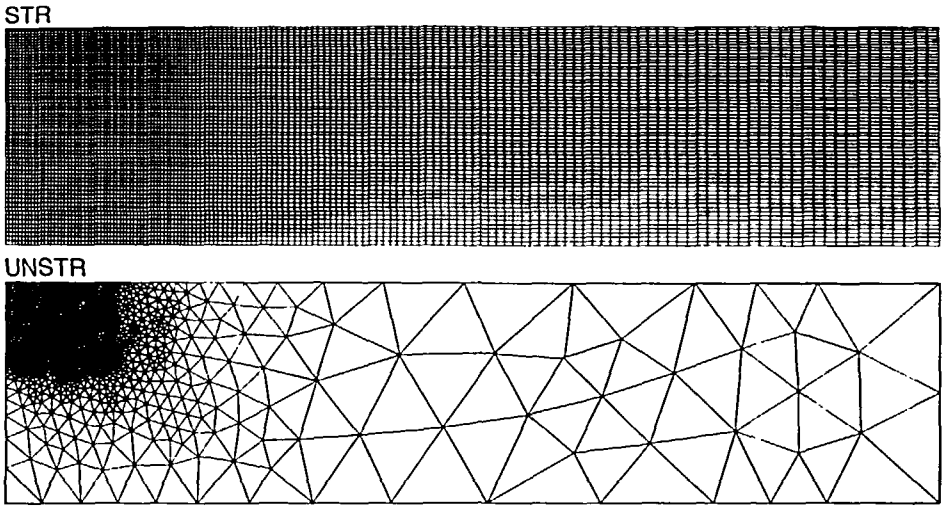

Figure 6 Meshes used in the calculation of the experiment. These meshes have the required refinement in the colder part for a proper simulation of blister growth

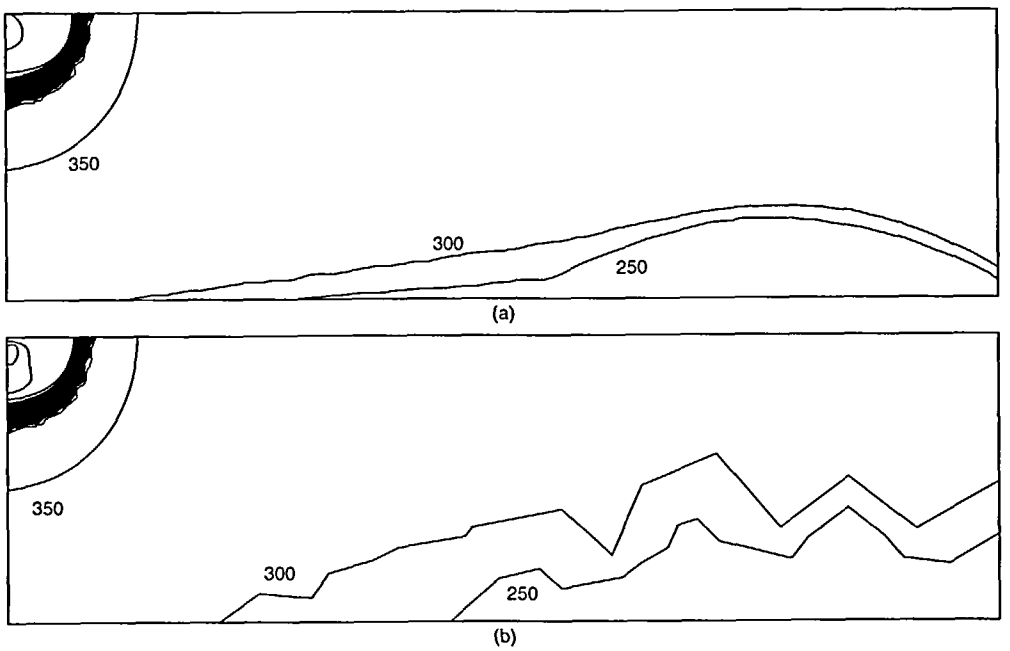

Figure 7 Numerical solutions of the problem at 6×10^5 sec. Contour levels: 250, 300, 350, 400 and 1,000-15,000ppm (the latter with intervals of 1,000ppm). A plateau of very high concentrations (> 12,000ppm) appears in the upper left corner, predicting a *blister* (pure δ-phase). The concentration changes abruptly from the blister to the bulk of the sample (notice the proximity of contours in the range 1,000-12,000 ppm). Most of the sample has concentrations between 300 and 400 ppm, corresponding to $\alpha + \delta$ co-existence. The proximity of the 250ppm and 300ppm contours evidences the boundary of a pure α-phase region that develops at the bottom right corner. The calculations allow for comparison between the structured (a) and unstructured (b) mesh

© Emerald Backfiles 2007

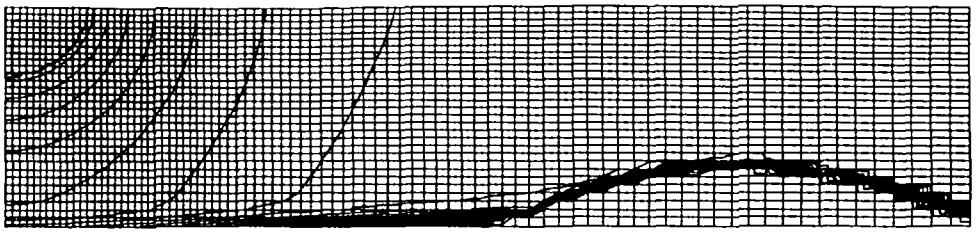

Figure 8 Numerical solution and mesh of the problem, using a coarse mesh. Contour lines from 150 to 450, at an interval of 10ppm. The 600ppm contour line is also plotted, corresponding to the curve at the upper left part. Notice that the contours follow the mesh only where the concentration gradient is very high, i.e. where the method approximates a discontinuity in the exact solution

be found in the finite-difference explicit numerical method proposed by Engström *et al.*[22] for diffusion of carbon in steel. There also exist semi-implicit schemes for the Stefan problem that can be shown to be related to the algorithm presented here[13,14,23]. We would like to point out that the essence of those algorithms can be understood from the picture we sketched in the section on the numerical method.

ACKNOWLEDGEMENTS

Fruitful discussions about the problem of hydrogen migration in zirconium with J.P. Abriata, J.C. Almagro, G. Domizzi and J. Ovejero-García are gratefully acknowledged. This work received sustained encouragement from the SUCAN group of CNEA. Mesh generation was performed with program ENREDO, kindly provided by E.A. Dari and M.J. Vénere. The help of E.A. Dari in solving the inverse thermal problem (*Figure 5*) and in many computational aspects of this work is also acknowledged. Our thanks to A. Larreteguy D. Zanette for carefully reading the manuscript, and to the reviewer for many valuable suggestions.

REFERENCES

1 Zuzek, E., Abriata, J.P., San Martín, A. and Manchester, F.D. *Binary Alloys Phase Diagrams*, 2nd ed, ASM International, Metals Park, OH (1990)
2 Erickson, W.H. and Hardie, D. The influence of alloying elements on the terminal solubility of hydrogen in α-zirconium, *J. Nucl. Mat*, **13**, 254-262 (1964)
3 Slattery, G.F. The terminal solubility of hydrogen in zirconium alloys between 30 and 400°C, *J. Inst. Metals*, **95**, 43-47 (1967)
4 Puls, M. The effect of misfit and external stresses on terminal solid solubility in hydride-forming metals, *Acta Metall.*, **29**, 1961-1968 (1981)
5 Qian, S. and Northwood, D.O. Hysteresis in metal-hydrogen systems: a critical review of the experimental observations and theoretical models, *Int. J. Hydrogen Energy*, **13**, 25-35 (1988)
6 Markowitz, J.M. The thermal diffusion of hydrogen in de alpha-delta Zircaloy-4, *Trans. Metall. Soc. AIME*, **221**, 819-824 (1961)
7 Sawatzky, A. and Vogt, E. Mathematics of the thermal diffusion of hydrogen in Zry-2, *Trans. Metall. Soc. AIME*, **227**, 918-928 (1963)
8 Sawatzky, A. Hydrogen in Zircaloy-2: Its distribution and heat of transport, *J. Nucl. Mat*, **2**, 321-328 (1960)
9 Byrne, T.P. and Léger, M. *Hydride Blister Growth Modeling*, Report Nr. 85-29-H (1985)
10 Enrique, R.A. Tesis de Licenciatura en Física, Instituto Balseiro, Bariloche, Argentina, 1994. In Spanish
11 Marino, G.P. Hydrogen supercharging in Zircaloy, *Mater. Sci. Eng.*, **7**, 335-341 (1971)
12 Byrne, T.P. *Hydride Precipitation and Blister Growth Modeling in Zr-Nb Pressure Tubes*, Report Nr. 84-30-H (1984)
13 Idelsohn, S.R., Storti, M.A. and Crivelli, L.A. Numerical methods in phase-change problems, *Arch. Comp. Met. Eng.*, **1**, 49-74 (1994)
14 Pham, Q.T. A fast, unconditionally stable finite-difference scheme for heat conduction with phase change, *Int. J. Numer. Meth. Eng.*, **28**, 2079-2084 (1985)

© Emerald Backfiles 2007

15 Domizzi, G., Enrique, R.A., Ovejero García, J. and Buscaglia, G.C. Blister growth in zirconium alloys: experimentation and modeling, *J. Nucl. Mat*, **229**, 36-47 (1996)
16 Buscaglia, G.C. and Saliba, R.O. Simulación de la migración de hidrógeno en aleaciones de circonio, *Rev. Int. Mét. Num. Cálc. Dis. Ing.* **8**, 395-406 (1992). In Spanish
17 Sawatzky, A. Formation of hydride blisters in Zirconium alloy pressure tubes, *Can. Metall. Q.* **24**, 227-234 (1985)
18 Enrique, R.A. and Buscaglia, G.C. *On Hydrogen Concentration Limits in Pressure Tubes: Improved Estimates*, Tech. Report CNEA-CAB 5501/95, Centro Atómico Bariloche, 1995
19 Freund, J. *A Model for Thermal Diffusion of Hydrogen in Zirconium Alloys*, Report 1992/32, Helsinki University of Technology, Institute of Mechanics (1992)
20 Jovanovic, M., Stern, A., Kneis, H., Weatherly, G.C. and Léger, M. Thermal diffusion of hydrogen and hydride precipitation in Zr-Nb pressure tube alloys, *Can. Metall. Q.* **27**, 323-330 (1988)
21 White, A.J., Sawatzky, A. and Woo, C.H. *A Computer Model for Hydride-blister Growth in Zirconium Alloys*, AECL Report 8386, Atomic Energy of Canada Limited (1985)
22 Engström, A., Höglund, L. and Ågreen, J. Computer simulation of diffusion in multiphase systems, *Metall. Trans. A*, **25A**, 1127-1134 (1994)
23 Amiez, G. and Gremaud, P.-A. On a numerical approach to Stefan-like problems, *Number. Math.* **59**, 71-89 (1991)

© Emerald Backfiles 2007